Network pharmacology of JAK inhibitors

Devapregasan Moodley[a], Hideyuki Yoshida[a], Sara Mostafavi[b,c], Natasha Asinovski[a], Adriana Ortiz-Lopez[a], Peter Symanowicz[d], Jean-Baptiste Telliez[d], Martin Hegen[d], James D. Clark[d], Diane Mathis[a,1], and Christophe Benoist[a,1]

[a]Division of Immunology, Department of Microbiology and Immunobiology, Harvard Medical School, Boston, MA 02115; [b]Department of Statistics, University of British Columbia, Vancouver, BC, Canada V6T 1Z4; [c]Department of Medical Genetics, University of British Columbia, Vancouver, BC, Canada V6T 1Z4; and [d]Inflammation and Immunology, Pfizer, Cambridge, MA 02139

Contributed by Christophe Benoist, June 24, 2016 (sent for review April 27, 2016; reviewed by Tadatsugu Taniguchi and Arthur Weiss)

Small-molecule inhibitors of the Janus kinase family (JAKis) are clinically efficacious in multiple autoimmune diseases, albeit with increased risk of certain infections. Their precise mechanism of action is unclear, with JAKs being signaling hubs for several cytokines. We assessed the in vivo impact of pan- and isoform-specific JAKi in mice by immunologic and genomic profiling. Effects were broad across the immunogenomic network, with overlap between inhibitors. Natural killer (NK) cell and macrophage homeostasis were most immediately perturbed, with network-level analysis revealing a rewiring of coregulated modules of NK cell transcripts. The repression of IFN signature genes after repeated JAKi treatment continued even after drug clearance, with persistent changes in chromatin accessibility and phospho-STAT responsiveness to IFN. Thus, clinical use and future development of JAKi might need to balance effects on immunological networks, rather than expect that JAKis affect a particular cytokine response and be cued to long-lasting epigenomic modifications rather than by short-term pharmacokinetics.

JAK inhibitor | tofacitinib | systems pharmacology

A drug's mechanism of action usually refers to the specific molecular or biologic activity that it perturbs, and drug optimization aims at maximizing potency and specificity vs. this target. However, the molecular target may be far removed from the processes that ultimately drive the therapeutic effect. For instance, even though the target is known, it remains unclear which cell or pathway is pivotally affected by anti-PD1 during cancer immunotherapy. Given the interdependencies of cellular and molecular players in biological systems, a drug is likely to have effects far broader than its molecular target. Conversely, it may be hampered by inherent resistance to perturbation of interconnected networks. This complexity is encapsulated in the concepts of network pharmacology, which proposes that drug development focus on network-level alterations, rather than on exquisite specificity for an individual target (1).

JAK kinase inhibitors (JAKis) have been intensively and successfully pursued over the last two decades (2, 3) and could be considered poster children of network pharmacology. JAK kinases (JAK1/2/3 and TYK2) are the initial mediators of signaling pathways triggered by many cytokines and hematopoietic growth factors, and activate transducers of the STAT family to prompt cell activation and phenotypic differentiation in all immunocyte lineages (4). The cytokine network is an unusually interconnected one, because cytokines can induce each other, or each other's receptors, and can enhance or stifle each other's signaling pathways. Further complexity stems from the widespread sharing of JAK kinases by cytokine receptors (e.g., JAK1 is connected to receptors for interferons, IL-2, -4, -6, -7, -9, -10, -11, -15, -21, and -27), and because most cytokine receptors are equipped with two different JAKs (e.g., JAK1 and JAK3 for IL-2R). Thus, even the most exquisitely specific JAK inhibitor (JAKi) will have pleiotropic effects that resonate through the immune system, affecting many cells and signals.

The therapeutic potential of inhibiting cytokine signaling in autoimmune diseases led to the development of first-generation JAKi (2, 3, 5), with good kinome-wide specificity, but shared cross-reactivity against several JAKs. Several proved to have clinical efficacy [e.g., against rheumatoid arthritis (RA), ulcerative colitis, psoriasis, or myeloproliferative diseases (6)]. They also have significant side effects that likely reflect cytokine blockade, such as bacterial and fungal infections, in particular, (re)activation of the varicella zoster virus, and at high doses, anemia and thrombocytopenia (2, 3). A new JAKi generation targets single JAK isoforms, which might improve adverse events by restricting the range of activity. Efficacy has been observed with JAK1-selective compounds (7) and compounds of reported specificity for JAK3 (ref. 8, but see ref. 2). However, the premise of substantially improved in vivo specificity remains unproven, because the impact of JAKi compounds on the immunological network is poorly understood.

Here, we explored the systemwide impact of JAKi by comprehensive immunologic and genomic profiling, comparing treatments with established pan-JAKi drugs to more recent isoform-specific inhibitors, making observations that provide important clues for future development and clinical application.

Results

Our immunogenomic explorations of JAKis used clinically efficacious doses of several compounds (Table S1). Two of them have cross-JAK activity and are already Food and Drug Administration-approved or in advanced clinical trials: Tofacitinib, a pan-JAKi (Tofa; aka CP-690,550), and Baricitinib, a JAK1/2 inhibitor (Bari; LY3009104) (2, 3). Two others have specificity for either JAK1 (PF-02384554; hereafter, JAK1i) or JAK3 (PF-06651600; JAK3i), with another JAK3-specific inhibitor in a few experiments (PF-06263313). This strategy discriminated between consequences of blocking one pathway and network-level effects resulting from a broader spectrum of activity or cascading effects through the cytokine network.

Significance

JAK kinase inhibitors (JAKis) have advanced options for treatment of autoimmune diseases. Because JAKs are signaling hubs for several cytokine receptors, JAKis' overall impact on the immune system and how they actually improve diseases like rheumatoid arthritis remain poorly understood. Combined immunophenotyping and genomic profiling revealed broad JAKi effects on the immunogenomic network, irrespective of inhibitor fine specificity, with effects on population homeostasis and coregulated gene-expression networks, particularly in innate immunocytes. Persistent repression by JAKis of IFN signature genes lasted beyond drug clearance and correlated with changes in the structure of the underlying chromatin, with direct implications for practical use of the drugs. Further JAKi development may need to take into account their broad network and epigenomic effects.

Author contributions: D. Moodley, J.-B.T., M.H., J.D.C., D. Mathis, and C.B. designed research; D. Moodley, H.Y., N.A., A.O.-L., and P.S. performed research; J.-B.T., M.H., and J.D.C. contributed new reagents/analytic tools; D. Moodley, H.Y., S.M., N.A., A.O.-L., P.S., J.-B.T., M.H., J.D.C., and C.B. analyzed data; and D. Moodley, D. Mathis, and C.B. wrote the paper.

Reviewers: T.T., The University of Tokyo; and A.W., University of California, San Francisco.

The authors declare no conflict of interest.

Data deposition: The data reported in this paper have been deposited in the Gene Expression Omnibus (GEO) database, www.ncbi.nlm.nih.gov/geo (accession no. GSE84568).

[1]To whom correspondence should be addressed. Email: cbdm@hms.harvard.edu.

This article contains supporting information online at www.pnas.org/lookup/suppl/doi:10.1073/pnas.1610253113/-/DCSupplemental.

Effects on JAKis on Immunophenotypes. We first assessed the impact of JAKi treatment on the size of the main immunocyte populations. JAKi were administered by oral gavage twice daily for 1 or 4 wk, at doses chosen to mimic clinical applications [average daily concentration equal to the concentration giving ~80% inhibition of IFN-α (JAK1i and pan-JAKi) or IL-15 (pan- and JAK3i) p-STAT signals in vitro]. Healthy and otherwise unperturbed mice were used to assess drug effects independent of modification of disease parameters in a disease model, much as one functionally evaluates disease susceptibility variants in healthy controls. Impact on immunocyte populations was assessed by flow cytometry of splenic populations, profiling the main lymphoid and myeloid cell types (salient results are provided in Fig. 1, and full results are provided in Fig. S1). Overall, there were no radical changes in cell pools, although small and reproducible adjustments did occur, most as soon as after 1 wk of treatment (all $P < 0.01$). Most affected were natural killer (NK) cells (Fig. 1*B*; mean fold change 0.3–0.7) and macrophages (MFs; Fig. 1*C*; mean fold change 0.3–0.6), the former consistent with previous clinical reports (9, 10). Adaptive lymphocytes did not change greatly overall, save for subtle redistributions of B-cell subsets (Fig. 1*A* and Fig. S1*C*) and a drop in Treg with JAK1i (Fig. S1*D*). These effects seemed mostly shared by all JAKis, suggesting a spread consistent with the range of cytokines affected and/or network-level adaptation.

Systemwide Genomic Effects on JAKis. We then performed gene-expression profiling to assess JAKi effects on the transcriptional network of immune cells, most broadly for B cells and MFs, representing lymphoid and myeloid lineages, but also including dendritic cells (DCs), polymorphonuclear neutrophils (GNs), NK cells, and CD4$^+$ T cells (T4; all together 238 datasets passing quality criteria, collated from several independent experiments). As described above, treatments lasted 1 wk, aiming at integrated effects on the immunogenetic network. As illustrated for Tofa effects in B cells and MFs (Fig. 2*A*), changes were mostly reductions in gene expression and relatively modest (very few transcripts reduced > twofold). This modest repressive effect was

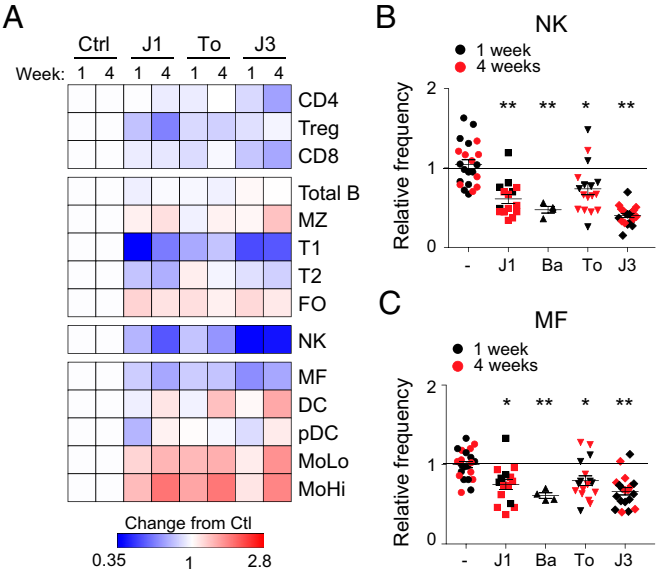

Fig. 1. Changes in immunocyte populations induced by JAKi treatment. Splenocyte profiles were assessed by flow cytometry after treatment with JAKi. Several experiments with treatments of 1 and 4 wk were combined. Values were normalized to the mean of vehicle-treated mice in the corresponding experiment. (*A*) Mean fold change for each cell type relative to its vehicle-treated control is represented on the heat map. (*B* and *C*) Data from several experiments are shown for NK cells (*B*) and macrophages (MF) (*C*). J1, JAK1i; Ba, Bari; To, Tofa; J3, JAK3i. *$P < 0.01$; **$P < 0.001$ Mann–Whitney u test).

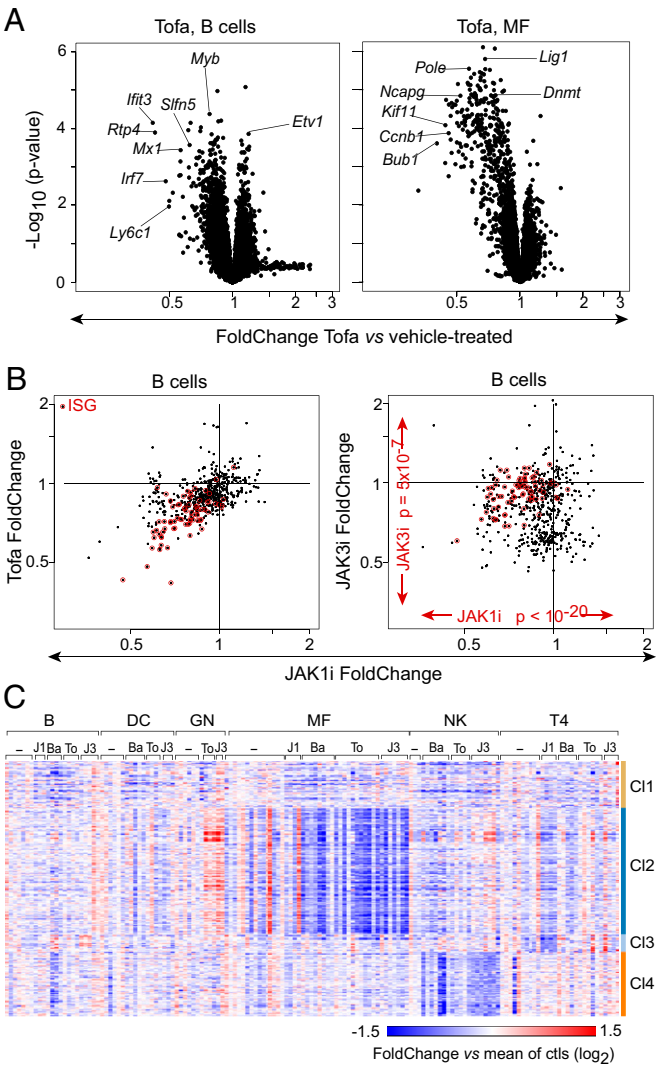

Fig. 2. Effects of JAK inhibition on the immunological transcriptome. Immunocytes were sorted from JAKi-treated mice (repeated dosing, twice daily, 1 wk), and mRNAs were profiled on genomewide microarrays. (*A*) Range and significance of changes: fold change vs. *P* value ("Volcano") plots for B cells (*Left*) and MF (*Right*) from Tofa-treated mice; all expressed genes are shown. (*B*) Drug specificity: fold change/fold change plot comparing effects of Tofa and JAK1i (*Left*) or Tofa and JAK3i (*Right*) in B cells. (*C*) Heat map of fold changes in the JAKi-affected gene set in six different splenic cell types, after treatment with different compounds (fold changes for each sample calculated vs. mean of all vehicle-treated samples). Cluster assignment is shown at right.

true in all cells examined and for monospecific-JAK as well as pan-JAK inhibitors (Fig. S1 *A* and *B*).

Because the drug effects on transcript levels were weak, we selected a set of 478 genes significantly [at false discovery rate (FDR) of 0.01] affected by any one drug in any one cell type. Of these effects, some were cell-type-specific, and others were ubiquitous. For instance, a gene cluster repressed by Tofa and by JAK3i in MFs was hardly affected in B cells (blue circle in Fig. S2*D*; see below for gene cluster details) and in most other cell types. However, a sizeable fraction of targets were affected in both cell types, in particular a set of IFN-responsive genes (ISGs; red in Fig. 2*B* and Fig. S2*D*). Transcripts for some characteristic Th cytokines showed a bias after JAK1i (*Ifng*, *Il10*, and *Il-2/21*, but not the *Il17* family), but not with other JAKi (Fig. S3), possibly reflecting a balancing consequence of multiple concurrent

inhibition (also, we cannot rule out unrecognized off-target activity of JAK1i).

In terms of drug specificity, some compound-preferential activities were observed, but many were shared. Indeed, it proved impossible to define "pure" JAK1i- or JAK3i-specific targets, because all JAK1i targets were affected in at least one cell type by JAK3i and vice versa, when the same fold-change and *P* value criteria were applied. Shared impact was expected between JAK1i and pan-JAKi (Fig. 2*B*, *Left*), but more surprising between JAK1i and JAK3i: Although JAKi-sensitive ISGs were more strongly affected by JAK1i, many were also depressed by JAK3i ($P = 5 \times 10^{-7}$; Fig. 2*B*, *Right*).

The heat map of Fig. 2*C* presents an overall perspective on the cell and drug specificity of the major affected clusters (discounting residual noise or unclustered effects; see also Fig. S4 and Dataset S1). Cluster 1 (Cl1) contains ISGs most strongly inhibited by JAK1i, but also by pan-JAKi compounds in all cell types. Cl2 transcripts (corresponding to the gene set circled in Fig. S2*D*) were predominantly affected in MFs, mainly by JAK3i and pan-JAKi, but were paradoxically enhanced by JAKi in GNs. Pathway analysis revealed Cl2 to be almost exclusively composed of cell growth-/cycle-related genes, indicating that JAKi compounds are affecting cell growth in MFs (consistent with their numeric drop above). A smaller cluster, Cl3, was predominantly affected in T4 by JAK1i, not enriched in any particular pathway or function (although it includes the coinhibitor *Pdcd1*). Finally, transcripts grouped in Cl4 were mainly affected by Bari and JAK3i in NK cells (again, with no standout pathways).

Such subtle and extended effects of JAKis and the difficulty in defining any compound-specific signature are consistent with the highly interconnected nature of the cytokine network perturbed by JAKis. To go beyond simple differential expression analysis and to derive the wider network effects of long-term JAK inhibition, we turned to network-based approaches, which evaluate changes in the correlation structure of the transcriptome (differential coexpression; DCE). The underlying principle is that DCE between a pair of genes reflects a modulation of the regulatory relationship between them, resulting from a different regulatory configuration in related, yet distinct, cell types (11) or from disease or drug treatment (12–14).

In practice, we followed two approaches. In the first, we computed pairwise DCE between the 478 affected genes defined above within 65 untreated datasets vs. 102 JAKi-treated samples. This comparison identified 101 gene pairs with significant DCE after Bonferroni correction (Fig. S5*A*). Most of these pairs lost correlation after treatment, but the relationship was strengthened for a few (blue and green in Fig. S5*A*). These pairs form distinct subnetworks (Fig. S5*B*) and are enriched for cell-cycle activators (in particular those regulating the G0/G1 transition), perhaps related to the loss of MFs.

Second, using a complementary approach that does not depend on structures within the data themselves, we assessed DCE within independently defined coexpression structures. We used the large collection of coregulated modules and predicted regulators derived by the Immunological Genome (ImmGen) consortium from coexpression during immunocyte differentiation (15). Projecting these module definitions onto the present data, we identified modules with a significant difference in coherence (defined as the ratio of intramodule to intermodule average correlation) in control or JAKi-treated samples. Here, a gain in coherence indicated coordinated activation/repression of a regulatory module and/or differential regulatory structure in control and treated conditions. Among the 81 ImmGen "coarse" modules, three (C19/62/74) showed a significant (FDR = 0.1) gain in coherence (Fig. 3*A*). These results were not driven by differences between compounds, because we observed similar effects when only Tofa-treated datasets were taken into account (Fig. S5*C*). C19 and C62 correspond mainly to genes preferentially expressed in NK cells and activated T cells in the ImmGen datasets (15) (Fig. 3*A*), and contain NK receptors and important cytokines and effectors (e.g., *Prf1*, *Gzmb/k*, *Ifng*, and *Csf2*). Although not identified individually

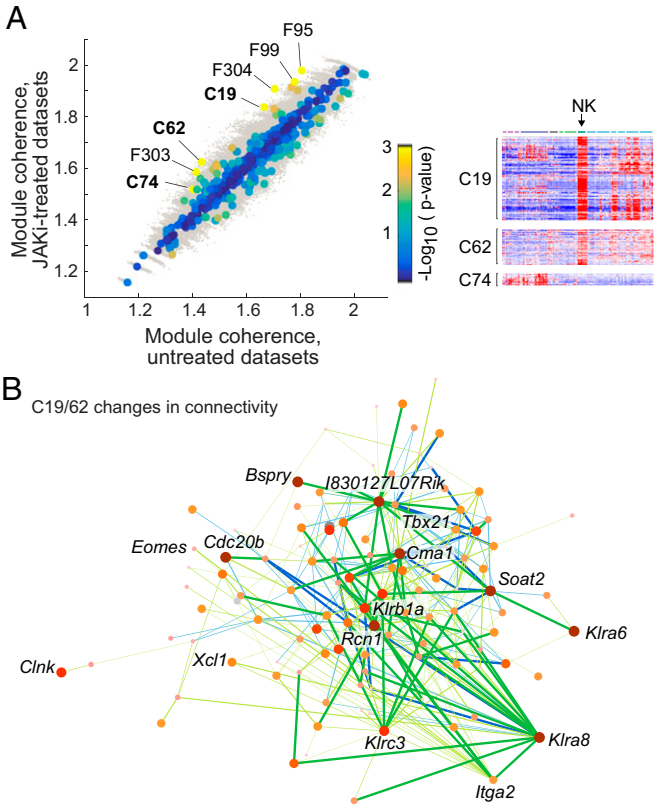

Fig. 3. JAKi-induced perturbations in the immunogenomic regulatory network. (*A*, *Left*) Coherence of coexpression modules (ImmGen) was computed in all untreated and treated datasets and compared. "C" and "F" refer to coarse or fine modules, respectively, as defined in ref. 15, and all F modules flagged here are actually components of the larger C19, C62, and C74 modules. Modules are color-coded according to the significance (log10 uncorrected *P* value) of the changes in coherence. Gray dots, coherence in randomly permuted datasets. (*A*, *Right*) Expression of genes from ImmGen modules C19, C62, and C74 across immunocyte cell types (ImmGen data). (*B*) Network representation of genes of ImmGen modules C16 and C62. Gain or loss of coexpression are shown in green and blue, respectively, and the genes are color-coded according to the number and significance of the changes in intramodule coexpression.

as differential, members of these modules showed modest down-regulation as a group in NK cells (Fig. S5*D*). Assessing the number of links that varied significantly (after correction for genomewide significance) showed that some genes in the C19/62 modules particularly contributed to the DCE (Fig. 3*B*), including several NK receptors of the *Klr* family [*Klrc3*, *Klrb1a*, and, most suggestively, *Klra8*, known to control responses to cytomegalovirus (16); Fig. S5*E*]. Thus, the network-based analyses highlighted a focusing and down-regulation of NK effector programs after JAKi treatment, which may be related to the phenotyping results.

JAKis Induce Stable Network Adaptation. These changes imparted by JAKis on immune cells and their genetic regulatory network resulted from cumulative effects over time. To determine which of these transcriptional changes corresponded to direct blockade of cytokine signaling vs. secondary adaptation, we compared gene-expression profiles generated after 1 wk of repeated treatment and drug washout and after a single acute administration 3 h before, when direct effects should be strongest (Fig. 4*A*). JAKi effects on the ISG cluster were clear after both chronic and acute treatments (Fig. 4*B*, *Left*), particularly for the subset of ISGs whose maintained expression was dependent on tonic IFN signals, which we recently showed to be the primary targets of the JAK1 blockade (17). In contrast, the "cell activation" cluster Cl2 repressed in MFs

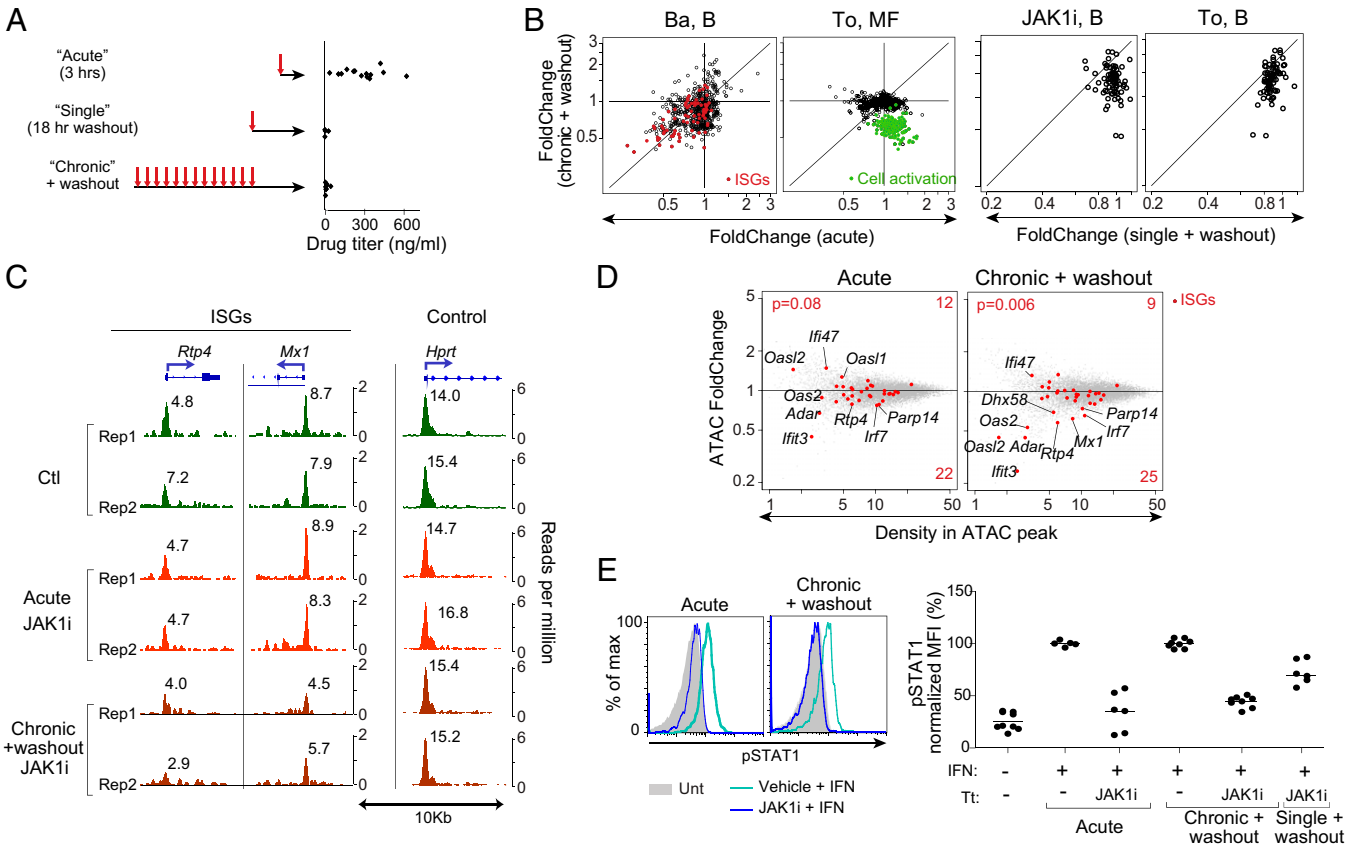

Fig. 4. Repeated JAK1i treatment leads to persistent effects on the ISG network. (*A*) Schematic representation of treatment protocol used to examine adaptive effects of JAK1i. Drug concentration in plasma at the end of each treatment are shown at right. (*B*) Gene expression profiling. (*B*, *Left*) Comparison of drug-induced changes in acute (*x* axis) vs. chronically (*y* axis) treated B cells showing ISGs (highlighted red) or MF cell activation/growth cluster (highlighted green). (*B*, *Right*) Comparison of drug-induced changes after a single treatment plus washout (*x* axis) vs. chronic treatment (*y* axis) also with washout per *A*, focusing on responsive ISGs. (*C*) B cells from mice treated with JAK1i per regimens in *A* were purified, and the genomewide landscape of accessible chromatin was determined by ATAC-seq (two replicates per condition). Representative ATAC-seq pileups around TSSs for tonic-sensitive ISGs are shown on the same scale for all profiles. (*D*) Genomewide changes in TSS ATAC-seq signals after JAK1i treatment, shown as ATAC-seq signal density (*x* axis) vs. fold change relative to vehicle (*y* axis) after acute (*Left*) or chronic (*Right*) treatment. Tonic-sensitive ISGs are shown in red. The count of genes with increased or decreased ATAC signal is shown (*P* value from a chi-square test vs. a random distribution). (*E*) Responsiveness to IFN signaling: B cells from acutely or chronically treated mice were challenged with IFN in vitro, and the resulting p-STAT1 was measured by flow cytometry. Phospho-STAT1 mean fluorescence intensity (MFI) was normalized to the mean of the IFN-only controls in each experiment (data pooled from two experiments).

by long treatment was unaffected at short times (Fig. 4*B*, *Left*). All of the JAKi compounds used here have relatively short half-lives (~1–2 h; Fig. S6*A*). Accordingly, repression of ISG expression had largely disappeared after a 16- to 18-h washout period after a single administration, for both the selective JAK1i and the pan-JAK inhibitor (Fig. 4*B*, *Right*). This comparison raised an important paradox: If the 16-h drug washout was sufficient to abolish transcriptional effects of one treatment, how could the chronic treatments described above, all of which included the same 16-h washout before profiling, show altered ISG expression? The implication was that repeated knockdown of tonic IFN signals by the drugs had a cumulative effect on the ISG network.

To elucidate the underlying mechanisms of this persistent transcriptional impact, we analyzed the state of the chromatin at the corresponding ISG loci, using assay for transposase-accessible chromatin with high-throughput sequencing (ATAC-seq) (18). We have recently shown that the acute response to IFN is accompanied by correlated changes in chromatin accessibility, reflected in the intensity of ATAC-seq signals in specific peaks around ISG transcriptional start sites (TSSs) or enhancer elements (17). Chromatin from splenic B cells was analyzed after acute or chronic treatment with JAK1i. The ATAC-seq profiles at TSS regions of two ISG loci (equally scaled in Fig. 4*C*) showed decreased chromatin accessibility after chronic treatment, but little or no change after acute treatment. This bias was generally true, as confirmed by quantitation of peak signals and calculation of a fold change relative to control-treated samples ($P = 0.006$ and 0.08 for chronic and acute treatments, respectively; Fig. 4*D*). As might be expected, those ISGs showing the strongest reduction in chromatin accessibility were also the most sensitive to IFN (Fig. S6*B*). We asked whether these persistent changes in chromatin structure also extended to responsiveness to IFN, assessed by induction of STAT1 phosphorylation 20 min after IFN challenge ex vivo. Indeed, mice subjected to long-term treatment showed reduced p-STAT1 responses to IFN (Fig. 4*E*). Thus, repeated dampening by JAK1i led to an adaptation of the IFN network, at the level of chromatin and of signaling pathways, that persisted even when the causal drug had essentially disappeared.

One Cytokine, Two JAKs: Similar Effects? An additional level of complexity in the JAK-controlled network is that signals from most cytokines involve two different JAKs (3). It is usually unclear whether both JAKs contribute, or whether each has distinct signaling and transcriptomic consequences (for instance, by triggering parallel signaling pathways) (19, 20). We addressed this question using the response of NK cells to IL-2 as a model. IL-2 binding to the low-affinity IL-2Rβγ receptor complex

expressed by NK cells (Fig. S7*A*) activates JAK1 and JAK3, which phosphorylate each other and STAT5, the key downstream transducer for IL-2 (21). Relative contributions of JAK1 and JAK3 to IL-2–induced responses are unclear (22, 23). IL-2 induced a robust response in primary NK cells ex vivo after 8 h of culture (Fig. S7*C*; listed in Dataset S2), which included a sizeable component of IFN-γ–sensitive genes (Fig. S7*D*), likely a secondary autocrine response, given the known induction of IFN-γ by IL-2 in NK cells (see also Fig. S7*H*) (24).

We first benchmarked the effects of selective JAK inhibition on IL-2 signaling by monitoring STAT5 phosphorylation (pSTAT5) in splenic NK cells ex vivo. JAK3i was more efficacious than JAK1i in this respect (Fig. 5*A* and Fig. S7*B*). We then compared the effects on the transcriptional response to IL-2 of inhibiting either JAK, with doses that yielded partial and comparable pSTAT5 inhibition, computing inhibition ratios (IL-2 + JAKi/IL-2 alone) for each drug. Transcripts repressed by IL-2 (defined in Fig. S7*C*) were equivalently de-repressed by both inhibitors (blue dots along the diagonal in Fig. 5*B*). However, there was a marked divergence in the capacity of JAK1i and JAK3i to block IL-2–induced transcripts (red dots). Many were equivalently repressed by both, but a distinct gene set was much more effectively repressed by JAK1i (orange and green circles in Fig. 5*B*; listed in Dataset S3). When the profiling was repeated with a wider dose range, the selective capacity of each inhibitor for these gene sets, still apparent at low or intermediate doses, converged at saturating doses (Fig. 5*C* and Fig. S7*E*).

Pathway analysis showed that JAK1i-preferential targets among IL-2–induced genes were mostly ISGs ($P = 10^{-22}$; Fig. S7*F*), whereas the common targets belonged to a network of STAT5-responsive genes ($P = 10^{-19}$), including cytokines/chemokine transcripts such as *Lif*, *Flt3lg*, or *Tnfrsf18*, and whose promoter regions were significantly enriched for the STAT5 motif (Fig. S7*G*). Taking pathway and motif enrichment results into account, we propose that the direct IL-2 signals were transduced equivalently through JAK1 and JAK3, whereas JAK1 partook more effectively in the secondary autocrine response to IL-2–induced IFN-γ (green traces in Fig. S7*E*), although JAK3i could eventually shut it down as well. Thus, JAK1i and JAK3i have unequal effects on IL-2–induced transcripts at pharmacologically relevant doses. One practical implication is that solely measuring changes in STAT phosphorylation provides an incomplete window on true compound activity. The results also explain the paradoxical effect of JAK3i on the ISG signature noticed in vivo. To answer the question posed at the onset, inhibitors of two different JAKs could indeed affect different facets of the response to a single cytokine, but with a dose-dependence (over a narrow range), which implies that fine consequences of JAKi treatment may shift over drug peaks and troughs in a treated individual.

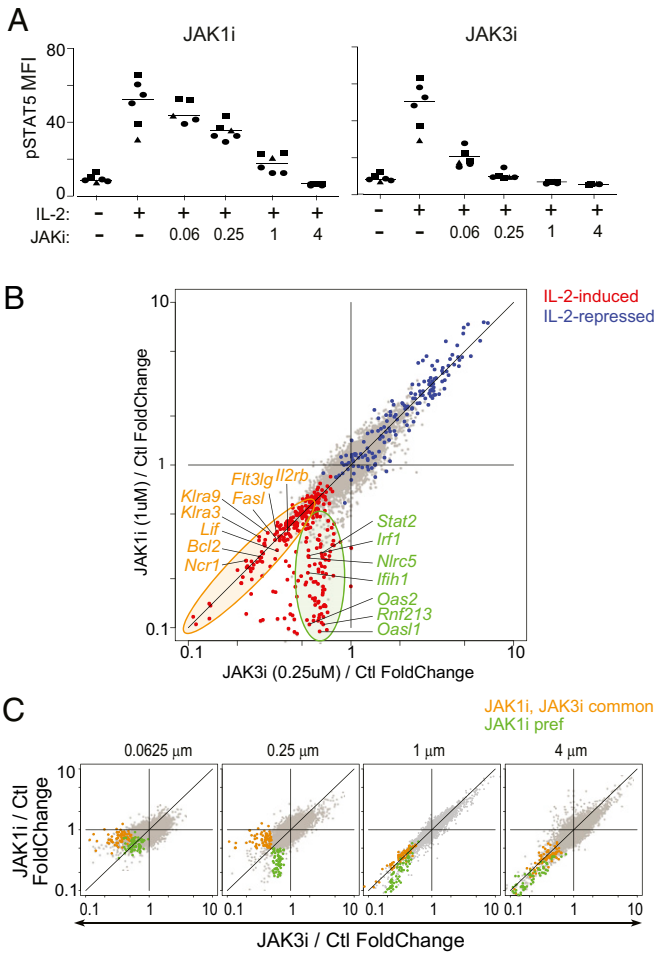

Fig. 5. Different effects of JAK1i and JAK3i on IL-2–induced transcripts. NK cells were purified by negative selection, activated IL-2 in vitro, alone or with graded concentrations of JAK1i or JAK3i. (*A*) Signal transduction from the IL-2 receptor evaluated by staining for phospho-STAT5. Different symbols indicate data from separate experiments. (*B*) Inhibition ratios (calculated as a ratio of expression values, JAKi+IL-2/IL-2) for JAK3i (*x* axis) and JAK1i (*y* axis); both JAKi at 0.25 μM. Red and blue highlights are transcripts induced or repressed by IL-2, respectively, as determined in Fig. S7. (*C*) Inhibition ratios at 0.25 μM JAKi in a first experiment were used to define JAK1i-preferred (green dots) and JAK1i/JAK3i-common effects (orange dots); these were then highlighted on similar JAK3i and JAK1i comparisons across a range of doses for each drug in a second experiment.

Discussion

Examining the impact of JAKi compounds on the immunogenomic network led to several major conclusions. First, whether on cells or genes, the effects are broad but subtle, overlapping between compounds, even those that target single JAK isoforms with high specificity. Second, the signaling and transcriptional network adapts to repeated JAK blockade, with the drug's effect persisting even after the compound has cleared. Third, when two JAK isoforms are involved in signals from a given cytokine, selectively blocking one or the other has a different impact on that cytokine's overall signature. These conclusions have direct and important implications for the use and future development of this class of drugs.

Because JAKs combinatorially route signals from many cytokine receptors, there was some expectation that their blockade would resonate through the immunogenomic network. These network effects were identifiable as clusters of genes flagged by traditional differential expression filters (Fig. 2), but other gene sets were spotted through changes in coexpression patterns within independently defined regulatory modules (Fig. 3). The latter finding indicated that JAKi treatments subtly rewire the regulatory connections within immunogenomic modules, and further illustrates the potential of network analyses to identify drug mechanisms (14), here flagging the NK receptor family for attention. Comfortingly, the strongest effects on the genomic network (cell growth transcripts in MF, effector functions in NK) corresponded to the most numerically perturbed immunocyte populations.

How do JAKis effectively improve RA and other autoinflammatory diseases? Previous suggestions included a suppression of pathogenic Th1/Th17 differentiation (7, 25) or a local effect on IFN and IL-6 signaling in RA joints (26). Our results flag innate cell populations as alternative or additional contributors. Effects in Th cells were modest, but the reduction in numbers and expression of activation clusters in MFs was suggestive, in light of their integrative role in destructive synovitis (27). Conversely, perturbations of NK cells, in numbers or in the wiring of their effector networks, support the notion that NK deficits underlie, at least in part, the viral reactivation events [noting that no correlation between changes in proportions of blood NK cells and infectious adverse events in patients has been observed (10, 28)]. Notably, *Klra8* [encodes Ly49h, intimately

involved in the response to mouse cytomegalovirus (16)] appeared as a differential hub in the network-level analysis, strongly suggesting that changes in NK receptors may be linked to JAKi adverse events involving large DNA viruses.

After the first generation of pan-JAKi drugs, the hope was that isoform-specific inhibitors might limit adverse risk profiles by narrowing cellular and molecular targets. However, we observed effects on cell homeostasis (NK and MF) in general with all JAKi, and even specific gene sets like ISGs were affected by all JAKi (Fig. 2*B*). This overlap is consistent with reported efficacy in early RA trials for both JAK1i and a reported JAK3i-biased inhibitor (8, 29, 30). There were, however, quantitative differences between signatures of isoform-specific JAKi (e.g., JAK1i remains more effective than JAK3i at inhibiting ISGs), and the comparative effect of JAK1i and JAK3i on the IL-2 response varies with dosage. Thus, one should not consider that isoform-specific JAKi will provide sharply delineated blockade of a specific pathway, but, rather, quantitative nuances of network-level effects, which may differentiate therapeutic windows relative to adverse events.

Adaptive resistance is defined as the state wherein biological systems (bacterial populations, tumors) become refractory to a drug through compensatory tuning of drug-affected pathways, often epigenetic. In the timeframe of our studies, the opposite occurred: Cumulative dampening of tonic signals by JAK1i and pan-JAKi drugs reset signaling pathways and chromatin structure such that they became refractory to further cytokine stimuli. ISG expression is maintained by tonic levels of IFN signals, partly triggered by commensal microbes (31), and involves several positive feedback loops (IFN induces STAT1/2). Thus, we propose that JAKi repression of tonic signaling blocks these feed-forward loops, the system rapidly turning into a low-responsive mode, a dampening amplified by the closing of accessible chromatin regions (circuits involving positive feedback overreact to dampening). This remnant dampening of IFN networks by JAKi is consistent with the clinical efficacy observed in regimens that include long daily periods with low drug presence, but may be a key contributor to viral reactivation. Operationally, these effects imply that choices of therapeutic dose and regimen should be less concerned with compound pharmacokinetics than with the persistent effects on the epigenetics of target networks.

Materials and Methods

JAKis were administered by oral gavage (0.5% methyl cellulose), twice daily to 5-wk-old C57BL/6J males (Jackson Laboratory) following Harvard Medical School Institutional Animal Care and Use Committee Protocol 02954. For systematic immunophenotyping by flow cytometry, splenocytes were stained with three antibody panels (lymphoid, myeloid, and B subsets; Table S2).

For ex vivo expression profiling, immunocytes were sorted to high purity. RNA was prepared and analyzed on microarrays per ImmGen SOP (www.immgen.org). Profiles were combined from experiments with 7–14 d of JAKi treatment, with drug effects quantified as mean FC between JAKi and vehicle, statistical significance estimated by *t* test FDR. Affected genes were filtered as mean FC vs. vehicle-treated <0.65 (or >1.8) with –log10(*P* value) >1.8 (FDR <0 .01) for any one cell type and any one drug, with CV across untreated <0.4. For DCE analysis, Pearson correlations between genes were computed to define two coexpression networks (from treated and untreated cells; Dataset S4) and *P* value [Bonferroni corrected (<5.0e-7)] for the difference in two corresponding coexpression values computed after Fisher's r-to-z transformation. Module coherence was computed for modules from Jojic et al. (15) (separately for vehicle- and JAKi-treated) as the ratio of average correlation between genes within the module and intermodule correlation, significance of the difference between coherence in control and treated samples computed by Monte Carlo permutation of treatment status. For chromatin accessibility, purified splenic B cells were used for ATAC-seq per ref. 17; the ∼10M unique reads/sample peaks identified by macs2 from merged datasets, and signal density in those 56,212 peaks computed in each dataset.

Detailed experimental procedures are shown in *SI Materials and Methods*.

ACKNOWLEDGMENTS. We thank N. Moret for insightful discussions and K. Hattori, C. Araeno, and A. Rhoads for assistance. This work was supported by a Pfizer, Inc., Sponsored Research Agreement.

1. Hopkins AL (2008) Network pharmacology: The next paradigm in drug discovery. *Nat Chem Biol* 4(11):682–690.
2. Clark JD, Flanagan ME, Telliez JB (2014) Discovery and development of Janus kinase (JAK) inhibitors for inflammatory diseases. *J Med Chem* 57(12):5023–5038.
3. Schwartz DM, Bonelli M, Gadina M, O'Shea JJ (2016) Type I/II cytokines, JAKs, and new strategies for treating autoimmune diseases. *Nat Rev Rheumatol* 12(1):25–36.
4. O'Shea JJ, Plenge R (2012) JAK and STAT signaling molecules in immunoregulation and immune-mediated disease. *Immunity* 36(4):542–550.
5. Kontzias A, Kotlyar A, Laurence A, Changelian P, O'Shea JJ (2012) Jakinibs: A new class of kinase inhibitors in cancer and autoimmune disease. *Curr Opin Pharmacol* 12(4):464–470.
6. Tefferi A (2012) JAK inhibitors for myeloproliferative neoplasms: Clarifying facts from myths. *Blood* 119(12):2721–2730.
7. Van Rompaey L, et al. (2013) Preclinical characterization of GLPG0634, a selective inhibitor of JAK1, for the treatment of inflammatory diseases. *J Immunol* 191(7):3568–3577.
8. Genovese MC, van Vollenhoven RF, Pacheco-Tena C, Zhang Y, Kinnman N (2016) VX-509 (Decernotinib), an oral selective JAK-3 inhibitor, in combination with methotrexate in patients with rheumatoid arthritis. *Arthritis Rheumatol* 68(1):46–55.
9. Schönberg K, et al. (2015) JAK inhibition impairs NK cell function in myeloproliferative neoplasms. *Cancer Res* 75(11):2187–2199.
10. Valenzuela F, et al. (2015) Effects of tofacitinib on lymphocyte sub-populations, CMV and EBV viral load in patients with plaque psoriasis. *BMC Dermatol* 15:8.
11. Ferraro A, et al. (2014) Interindividual variation in human T regulatory cells. *Proc Natl Acad Sci USA* 111(12):E1111–E1120.
12. Bandyopadhyay S, et al. (2010) Rewiring of genetic networks in response to DNA damage. *Science* 330(6009):1385–1389.
13. Zhang B, et al. (2013) Integrated systems approach identifies genetic nodes and networks in late-onset Alzheimer's disease. *Cell* 153(3):707–720.
14. Woo JH, et al. (2015) Elucidating compound mechanism of action by network perturbation analysis. *Cell* 162(2):441–451.
15. Jojic V, et al.; Immunological Genome Project Consortium (2013) Identification of transcriptional regulators in the mouse immune system. *Nat Immunol* 14(6):633–643.
16. Arase H, Mocarski ES, Campbell AE, Hill AB, Lanier LL (2002) Direct recognition of cytomegalovirus by activating and inhibitory NK cell receptors. *Science* 296(5571):1323–1326.
17. Mostafavi S, et al.; Immunological Genome Project Consortium (2016) Parsing the interferon transcriptional network and its disease associations. *Cell* 164(3):564–578.
18. Buenrostro JD, Giresi PG, Zaba LC, Chang HY, Greenleaf WJ (2013) Transposition of native chromatin for fast and sensitive epigenomic profiling of open chromatin, DNA-binding proteins and nucleosome position. *Nat Methods* 10(12):1213–1218.
19. Stark GR, Darnell JE, Jr (2012) The JAK-STAT pathway at twenty. *Immunity* 36(4):503–514.
20. Villarino AV, Kanno Y, Ferdinand JR, O'Shea JJ (2015) Mechanisms of Jak/STAT signaling in immunity and disease. *J Immunol* 194(1):21–27.
21. Boyman O, Sprent J (2012) The role of interleukin-2 during homeostasis and activation of the immune system. *Nat Rev Immunol* 12(3):180–190.
22. Haan C, et al. (2011) Jak1 has a dominant role over Jak3 in signal transduction through γc-containing cytokine receptors. *Chem Biol* 18(3):314–323.
23. Zhou YJ, et al. (2000) Hierarchy of protein tyrosine kinases in interleukin-2 (IL-2) signaling: Activation of syk depends on Jak3; however, neither Syk nor Lck is required for IL-2-mediated STAT activation. *Mol Cell Biol* 20(12):4371–4380.
24. Kubota A, Lian RH, Lohwasser S, Salcedo M, Takei F (1999) IFN-gamma production and cytotoxicity of IL-2-activated murine NK cells are differentially regulated by MHC class I molecules. *J Immunol* 163(12):6488–6493.
25. Ghoreschi K, et al. (2011) Modulation of innate and adaptive immune responses by tofacitinib (CP-690,550). *J Immunol* 186(7):4234–4243.
26. Boyle DL, et al. (2015) The JAK inhibitor tofacitinib suppresses synovial JAK1-STAT signalling in rheumatoid arthritis. *Ann Rheum Dis* 74(6):1311–1316.
27. Roberts CA, Dickinson AK, Taams LS (2015) The interplay between monocytes/macrophages and CD4(+) T cell subsets in rheumatoid arthritis. *Front Immunol* 6:571.
28. American College of Rheumatology (2014) 2014 ACR/ARHP Annual Meeting abstract supplement. *Arthritis Rheumatol* 66(Suppl 10):S1–S1402.
29. Fleischmann RM, et al. (2015) A randomized, double-blind, placebo-controlled, twelve-week, dose-ranging study of decernotinib, an oral selective JAK-3 inhibitor, as monotherapy in patients with active rheumatoid arthritis. *Arthritis Rheumatol* 67(2):334–343.
30. American College of Rheumatology (2015) 2015 ACR/ARHP Annual Meeting abstract supplement. *Arthritis Rheumatol* 67(Suppl 10):1–4046.
31. Abt MC, et al. (2012) Commensal bacteria calibrate the activation threshold of innate antiviral immunity. *Immunity* 37(1):158–170.
32. Benjamini Y, Hochberg Y (1995) Controlling the false discovery rate: A practical and powerful approach to multiple testing. *Roy Stat Soc B* 57:289–300.
33. Zhang Y, et al. (2008) Model-based analysis of ChIP-Seq (MACS). *Genome Biol* 9(9):R137.

Supporting Information

Moodley et al. 10.1073/pnas.1610253113

SI Materials and Methods

Mice and Treatments. C57BL/6J (5- or 6-wk-old males) were purchased from the Jackson Laboratory and maintained in a specific pathogen-free facility at Harvard Medical School (Institutional Animal Care and Use Committee Protocol 02954). JAKis were administered by oral gavage, in 0.5% methyl cellulose, twice daily for all long-term treatments. Doses used were PF-6647511(JAK1/2), 5 mg/kg; CP-690550–10(Pan), 25 mg/kg; PF-02384554(Jak1), 100 mg/kg; PF-06263313(JAK3), 100 mg/kg; and PF-06651600(JAK3), 20 mg/kg.

Immunocyte Phenotyping. Splenocytes from treated and control mice were prepared by mechanical disruption through a cell strainer. Red blood cells were lysed on ice with ammonium-chloride-potassium lysing buffer (Lonza 10-548E). Cells were washed and stained with three different antibody panels for a systematic evaluation of immunocyte composition (Table S2). Antibodies were purchased from BioLegend (unless otherwise stated). For intracellular staining, cells were first stained for surface markers, then fixed and permeabilized with 1× fixation/permeabilization (fix/perm) buffer (eBioscience 00-8222) overnight at 4 °C, then stained in 1× fix/perm buffer for 1 h at 4 °C. Labeled cells were analyzed on a BD LSRII, and analysis was performed with FlowJo (TreeStar) software.

Immunocyte Fractionation and in Vitro Challenge. Splenocytes were prepared from spleens of 6- to 8-wk-old C57BL/6 mice by mechanical dissociation. Splenic NK cells were isolated by negative selection (Stemcell Technologies; EasySep kit 19855), washed, and cultured at 37 °C in RPMI 1640 supplemented with 10% (vol/vol) FBS, L-glutamate, and penicillin/streptomycin in round-bottom 96-well plates at 10^5 cells per well. Culture plates were prepared with 250 U/mL recombinant mouse IL-2 (Peprotech 212-12) and either JAK1i or JAK3i at a fourfold dose range (0.0625, 0.25, 1, and 4 μM) in 2% (vol/vol) DMSO, before addition of cells. NK cells were cultured in vitro for 8 h and thereafter transferred directly into TRIzol to extract RNA for gene expression profiling.

For phospho-STAT5 experiments, 15 min after culture, cells were fixed in 2% paraformaldehyde for 20 min at room temperature (RT). Thereafter cells were permeabilized overnight with 90% methanol at −20 °C and then stained with anti-pSTAT5 (eBiosciences 17-9010-42) on ice for 30 min.

To test IFN responsiveness, splenic B cells were isolated by negative selection (Stemcell Technologies; EasySep kit 19854) and cultured with 100 U/mL IFN-α (R&D Systems 12100-1) for 20 min. Cells were then fixed in 2% paraformaldehyde for 20 min at RT. Thereafter, cells were permeabilized overnight with 90% methanol at −20 °C and then stained with anti-pSTAT1 (BD Biosciences 612564) on ice for 30 min.

Gene Expression Profiling. For in vivo profiling, immunocytes from treated mice were sorted to high purity by flow cytometry according to ImmGen standard operating procedures (www.immgen.org). In practice, splenocytes were size (scatter) and singlet gated, stained with propidium iodide for viability, and sorted as follows: B, PI^- $TCR\beta^-$ $CD19^+$; DC, $PI^-CD19^-CD3^-CD11c^+MHCII^+$; GN, $PI^-CD19^-CD3^-CD11c^-MHCII\text{-}Ly6G^+$; NK, PI^- $TCR\beta^-$ $CD19^+NK1.1^+$; and T4, PI^- $TCR\beta^+$ $CD19^-$ $CD4^+$. For MFs, cells from peritoneal lavage, gated for size, singlet, and viability, were sorted as $PI\text{-}F4/80^+ICAM2^+$.

Two successive sorts were performed for optimal purity, the second yielding 50×10^3 cells directly into TRIzol. For profiling after in vitro culture, cells were spun down by centrifugation at $500 \times g$ for 5 min and taken up in TRIzol. RNA was prepared from these TRIzol lysates and used for gene expression profiling on Affymetrix MoGene ST1.0 microarrays (Expression Analysis). After normalization with the RMA algorithm, data were preprocessed by removing unexpressed probes, discarding transcripts with high interreplicate coefficient of variation (typically Sno loci), and by using residuals from a linear model fit to the sample's dynamic range (to smooth artifactual variance due to different signal intensities, which can become an issue in cases of low true variance).

Evaluation of Drug Effects: Genomics. Gene expression profiles were combined from several individual experiments (n = 3–7 per group, more than two to seven independent experiments) involving paired JAKi- or vehicle-treated mice. Unless otherwise specified, treatments ranging from 7 to 14 d were combined, because effects were comparable with respect to JAKi target inhibition. Drug effects were quantified, independently for each drug and each cell type, as the mean fold change between JAKi- and vehicle-treated mice, estimating statistical significance by a simple t test, controlled for multiple sampling by computing a Benjamini–Hochberg FDR (32).

Because the drug effects on transcript levels were weak, we reduced noise and false positives by selecting a set of affected genes that had, for any one cell type and any one drug, a fold change relative to untreated of 0.65 (or >1.8) or less and –log10(P value) >1.8 (FDR < 0.01), combined with a CV across untreated <0.4. This selection yielded 496 down-regulated and 56 up-regulated probes, corresponding to 433 and 56 unique genes, respectively, or 478 genes when combined.

DCE Analysis. Two coexpression networks (using Pearson correlation) were defined across the 478 differentially expressed genes (Dataset S3) by using data from all experiments (65 control and 125 Jak treatment experiments). For the Jak-treated samples, we only considered long-term treated samples (defined as more than two treatments). A P value for the difference in two corresponding coexpression values (comparing one from baseline and one from treated samples) was computed after performing Fisher's r-to-z transformation. The P values were corrected by using the Bonferroni correction (<5.0e-7).

Module-Based Differential Coherence. We used the module definitions provided by Jojic et al. (15). Only modules that contained four or more genes were considered, resulting in 388 assessed modules. The module coherence measure (per module) was computed as the ratio of average correlation between expression levels of genes within the module over the average correlation of the module's mean with other modules' means (intermodule correlation). This coherence metric was separately computed by using the control and Jak-treated samples. Significance of the difference between coherence in control and treated samples was computed by using permutation analysis (permutation of treatment status).

Chromatin Accessibility (ATAC-seq). ATAC-seq libraries were constructed by following Buenrostro et al. (18), as reported (17). Briefly, splenic B cells were isolated by negative selection (Stemcell Technologies; EasySep kit 19854) from 6-wk-old C57BL/6J male mice after JAKi (3404) treatments designated in

Fig. 5*A* (acute, 3 h after a single oral gavage; chronic, twice daily for a week and 18-h washout after the last treatment; and control, 3 h after a single oral gavage of vehicle), and ∼50,000 cells were used to construct the libraries using Nextera DNA Sample Prep Kit (Illumina), which were sequenced on an Illumina HiSeq2500 for 50-bp, single-end in a rapid run mode (18∼28M reads for each). After trimming low quality reads by sickle1.2 (https://github.com/najoshi/sickle) and adapter sequence by cutadapt1.2.1, short reads were mapped to mm10 by bowtie1.1.1 with –m 1 option to avoid nonunique alignments. Then, reads mapped to mitochondrial DNA (30.1 to ∼42.9%) and duplicated reads (28.1 to ∼39.4%) were removed to retain 9.2∼12.0M unique reads for each. The aligned results from the same condition were merged by samtools merge, and peaks were determined by macs applying options–nomodel–shift 5–extsize 170–keep-dup 2–SPMR -q 0.01 (samtools1.1 and macs2.1.0) (33). Identified peaks from three conditions were merged by BEDTools mergeBed (46,273 peaks from control, 51,654 peaks from acute, and 49,731 peaks from chronic) to isolate 56,212 merged peaks, and the reads within these peaks were counted from each aligned result before merging by BEDTools coverageBed (BEDTools2.19.0). Read counts were normalized by quantile-normalization and region length to calculate signal densities for each peak, of which 10,124 peaks overlapping TSSs of refGenes (downloaded from University of California, Santa Cruz; genome.ucsc.edu) were used to plot the ATAC-seq signals. To visualize the representative ATAC-seq signals, pileup outputs from macs were normalized by quantile normalization taking every 10-bp bin, converted into bigwig format, and visualized by IGV software.

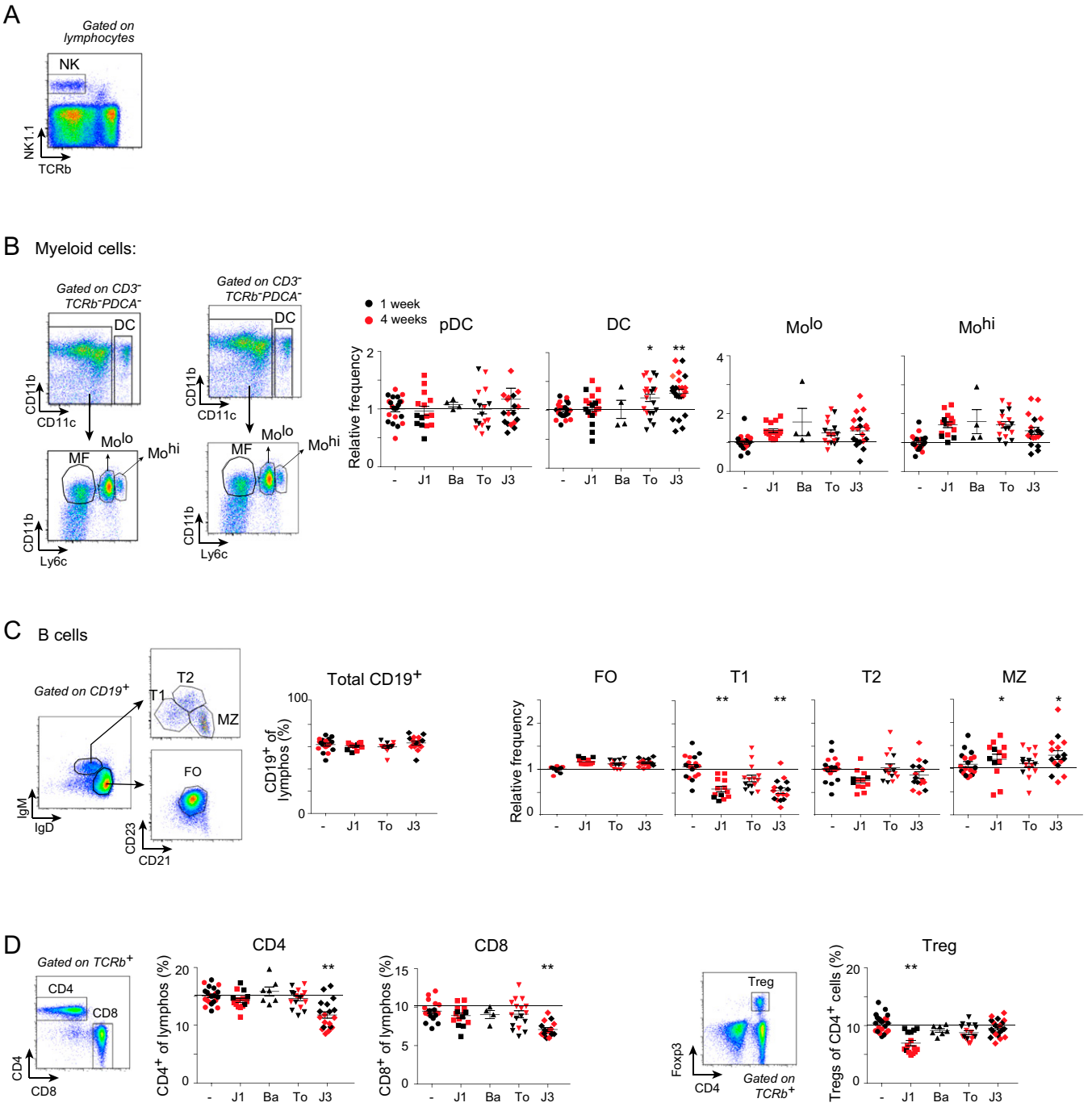

Fig. S1. Changes in immunocyte populations induced by JAKi treatment. Splenocyte profiles were assessed by flow cytometry after treatment with JAKi. Representative profiles and gating strategy are shown. J1, JAK1i; Ba, Bari; To, Tofa; J3, JAK3i. (*A*) Gating strategy for NK cells. (*B*) Myeloid cells: DCs and Ly6clow or high monocytes; several experiments with treatments of 1 and 4 wk (in red) are combined, and values are shown normalized to the mean of vehicle-treated mice in the corresponding experiment. (*C*) B lymphocytes and subsets thereof. FO, follicular B cells; MZ, marginal zone B cells; T1, T2, transitional B cells. (*D*) $CD4^+$ and $CD8^+$ T (as proportion of total lymphocytes) and $FoxP3^+$ Tregs (as proportion of CD4+ T cells). $*P < 0.01$; $**P < 0.001$ (Mann–Whitney *u* test).

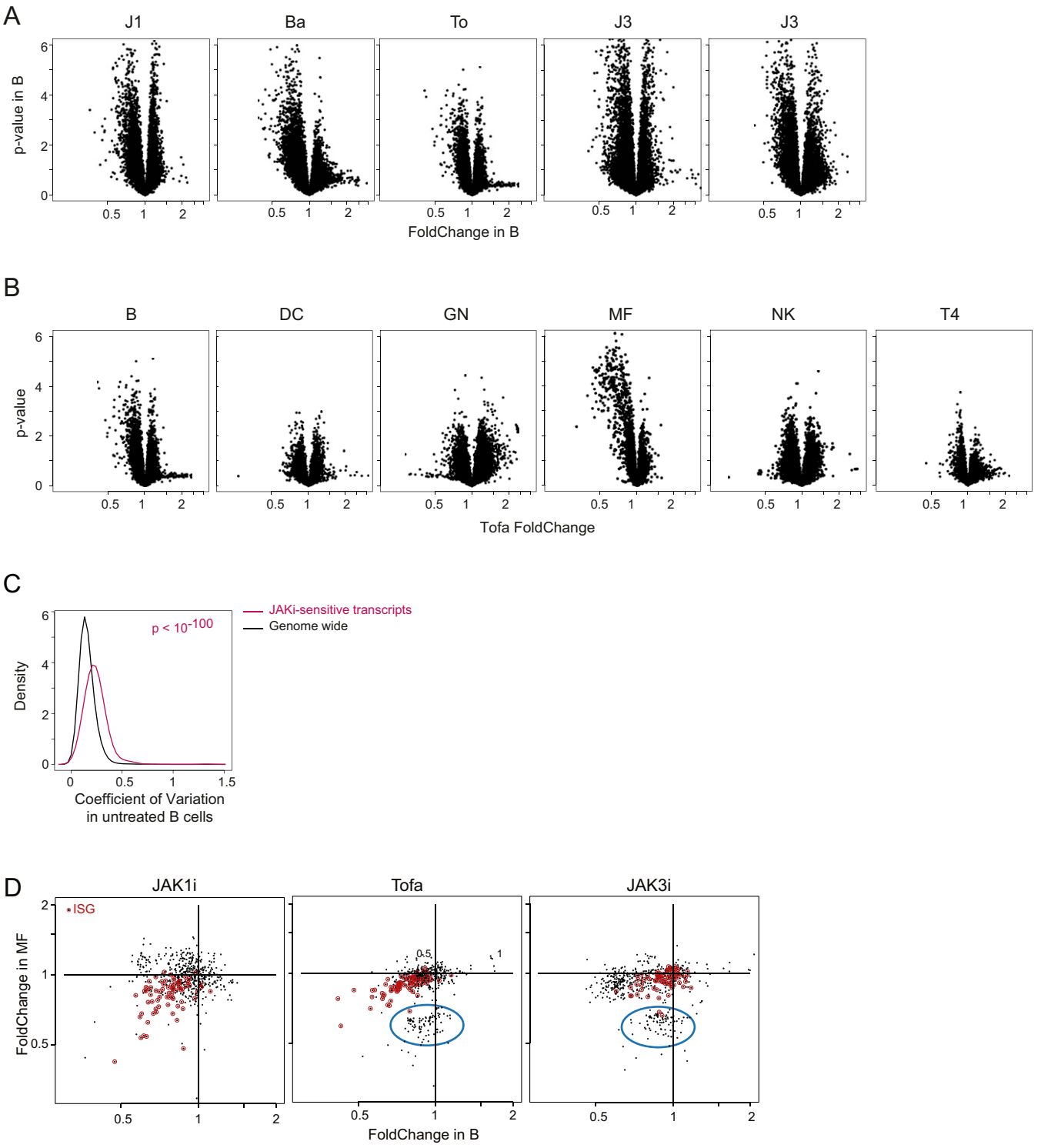

Fig. S2. Effects of JAK inhibition on immunocyte transcriptomes. Mice were treated with pan- and monospecific-JAKi twice daily for 1 wk. Immunocytes were sorted from these and mRNAs profiled on genomewide microarrays. (*A*) Range and significance of changes for all inhibitors in B cells. Volcano plots (fold change vs. *P* value) for all expressed genes are shown. (*B*) Immunocyte-specific effects in Tofa-treated mice. Volcano plots (fold change vs. *P* value) for all expressed genes in each immunocyte population are shown. (*C*) Transcript variability at baseline; distribution of coefficient of variation for genomewide and JAKi-sensitive transcripts in untreated B cells. (*D*) Cell specificity: fold change/fold change plot comparing drug-induced changes in B cells vs. MF (only the 478 set of affected genes is shown). IFN signature genes are highlighted in red, and cell growth-/cycle-related genes are circled in blue.

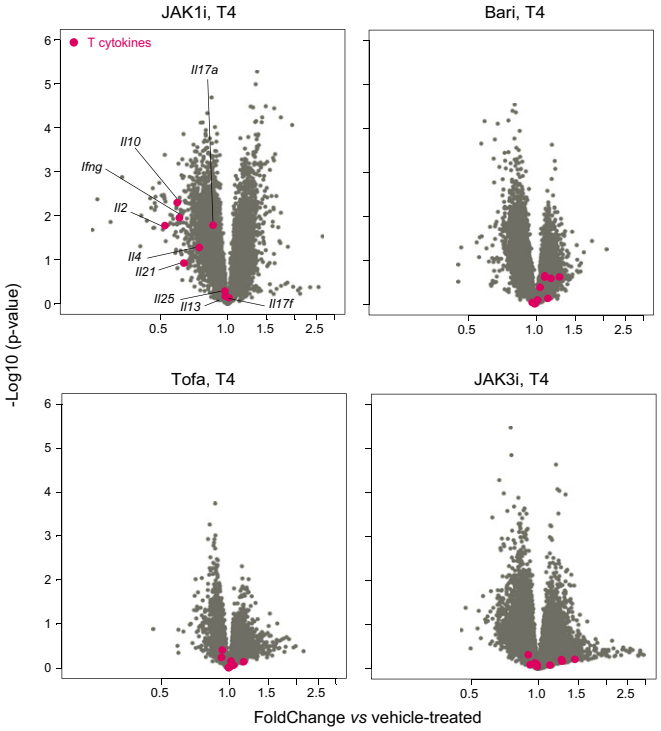

Fig. S3. Effects of JAK inhibition on Th cytokine expression. T4 cells from mice treated with pan- and monospecific-JAKi were sorted, and mRNAs were profiled by genomewide microarrays. Volcano plots (fold change vs. *P* value) for all genes expressed in treated T4 cells are shown, with Th cytokines highlighted in red.

Cluster 1

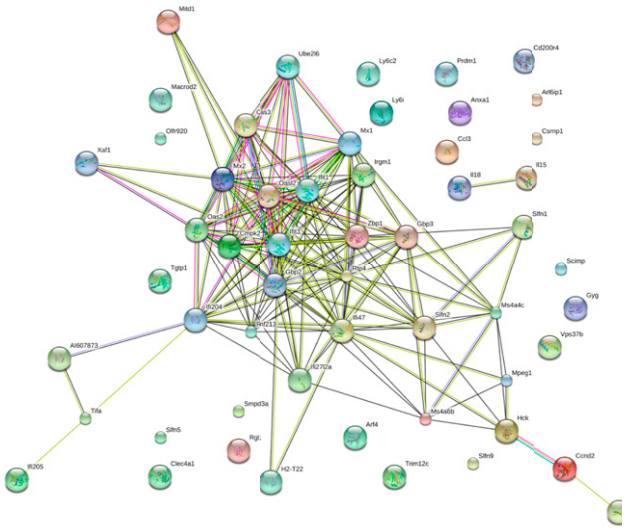

Gene Set Name	p-value	FDR q-value
Interferon alpha response	1.79×10^{-12}	4.48×10^{-11}
Interferon gamma response	6.65×10^{-22}	3.33×10^{-20}
Allograft rejection	2.29×10^{-5}	3.81×10^{-4}

Cluster 2

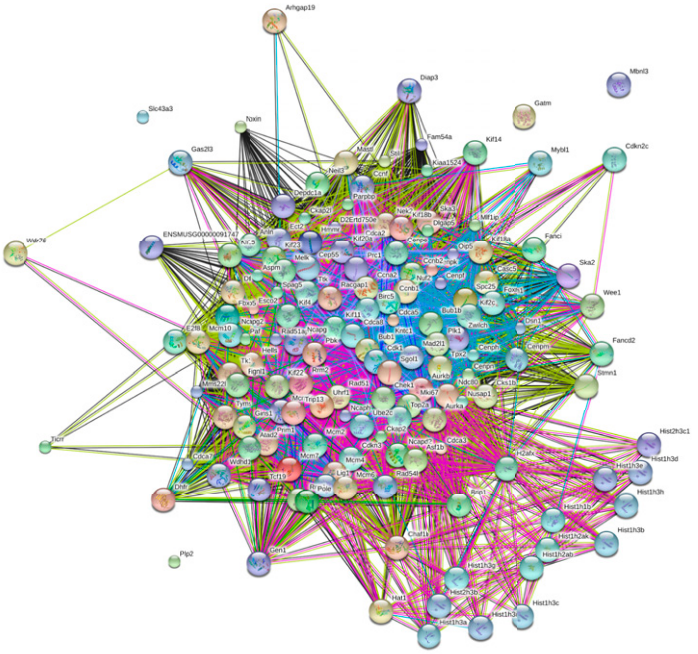

Gene Set Name	p-value	FDR q-value
E2F targets	4.7410^{-87}	2.37×10^{-85}
G2M Checkpoint	1.24×10^{-69}	3.11×10^{-68}
Mitotis spindle	2.36×10^{-36}	3.93×10^{-35}

Cluster 3

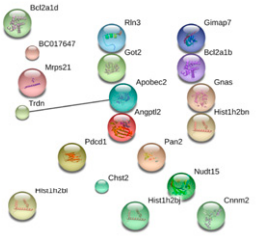

Cluster 4

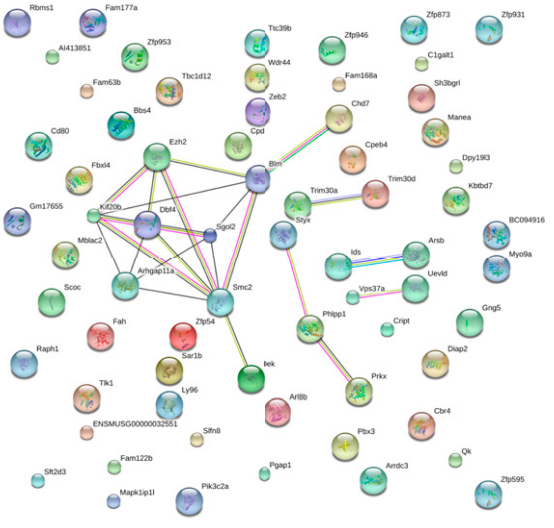

Gene Set Name	p-value	FDR q-value
G2M Checkpoint	1.07×10^{-4}	5.35×10^{-3}

Fig. S4. Network and pathway analysis of JAKi-sensitive clusters. JAKi-sensitive genes were assigned to four clusters (per Fig. 2*C*). Functional interactions among genes in each cluster were examined by using STRING software. Pathway enrichment for genes in each cluster was performed by querying hallmark gene sets in the Molecular Signatures Database (Version 5.1; software.broadinstitute.org/gsea/msigdb/).

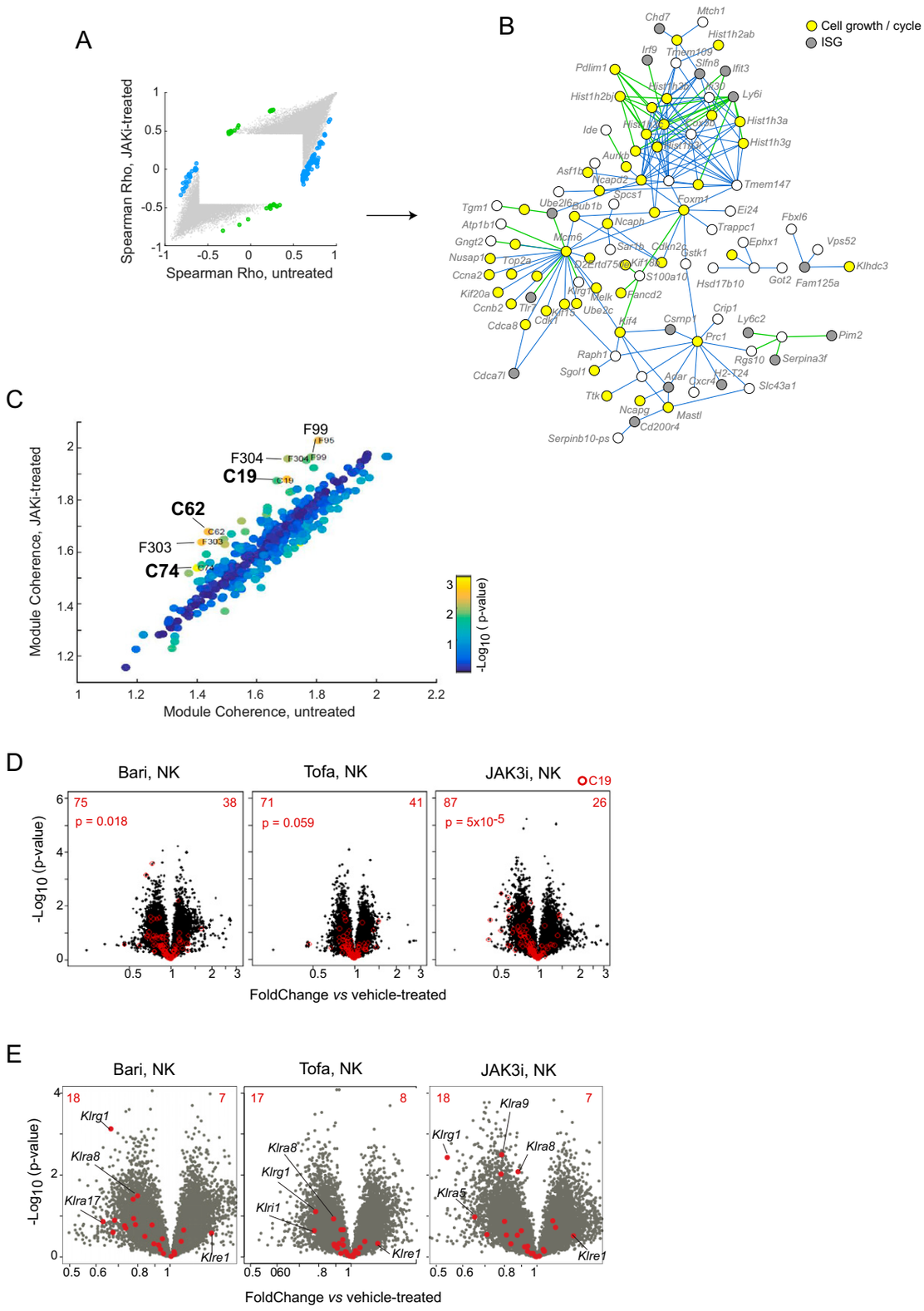

Fig. S5. Effects of JAK inhibition on ImmGen regulatory modules. (*A*) Coexpression in gene pairs (Spearman's rho) was computed in the untreated and the JAKi datasets and compared. Gene pairs with significant DCE were identified by computing Fisher's r-to-z transformation and assessing the significance of the two transformed coefficients using a z-test; Bonferroni correction was used to correct for multiple testing (number of links per edges); significant differences are shown in green or blue when increased or decreased, respectively. (*B*) Changed coexpression networks for genes with significant DCE (defined in *A*). Only significant differential coexpressed links (Bonferroni correction) are shown. Links between genes that gain or lose coexpression after treatment are shown in green and blue, respectively. (*C*) Coherence of previously determined coexpression modules (ImmGen) was computed in Tofa-treated and untreated datasets and compared. "C" and "F" modules refer to coarse or fine modules as defined {9457}. Modules are color-coded according to the significance (Bonferroni-corrected) of the changes in coherence. Gray dots: coherence in randomly permuted datasets. (*D* and *E*) Volcano plots (fold change vs. *P* value) for NK cells from JAKi-treated mice showing down-regulation of ImmGen regulatory module C19 (*D*) and *Klr* family genes highlighted in red (*E*).

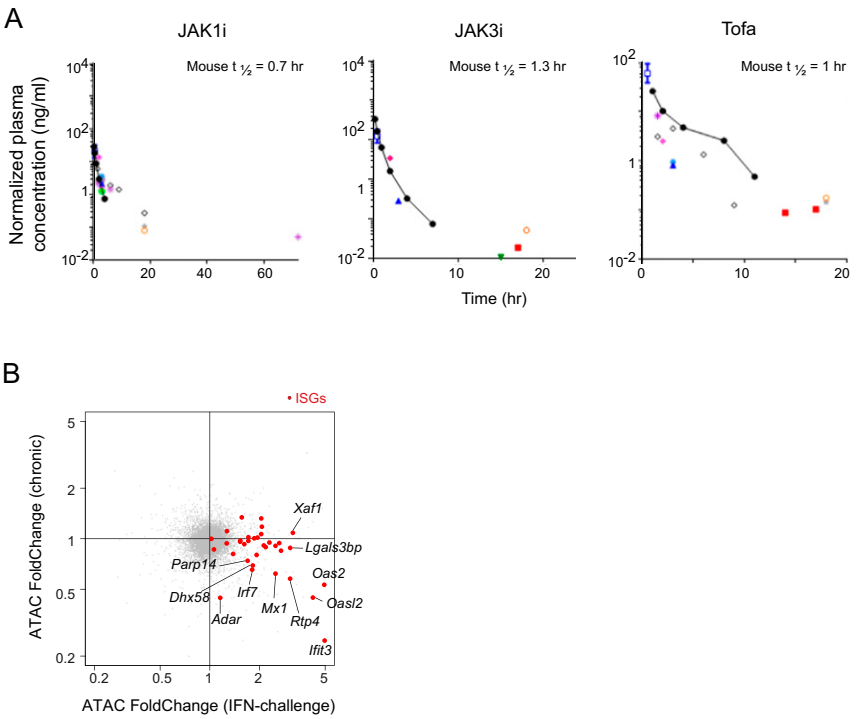

Fig. S6. JAKi clearance in mice. Plasma was collected from mice treated with JAKi at various time points, and residual level of inhibitor was measured. (*A*) Normalized plasma concentration and half-life of JAKi. Different symbols show data from separate experiments and correspond to data described above. (*B*) Comparison of ATAC fold change resulting from acute IFN treatment (*x* axis) vs. chronic JAK1i treatment (B cells).

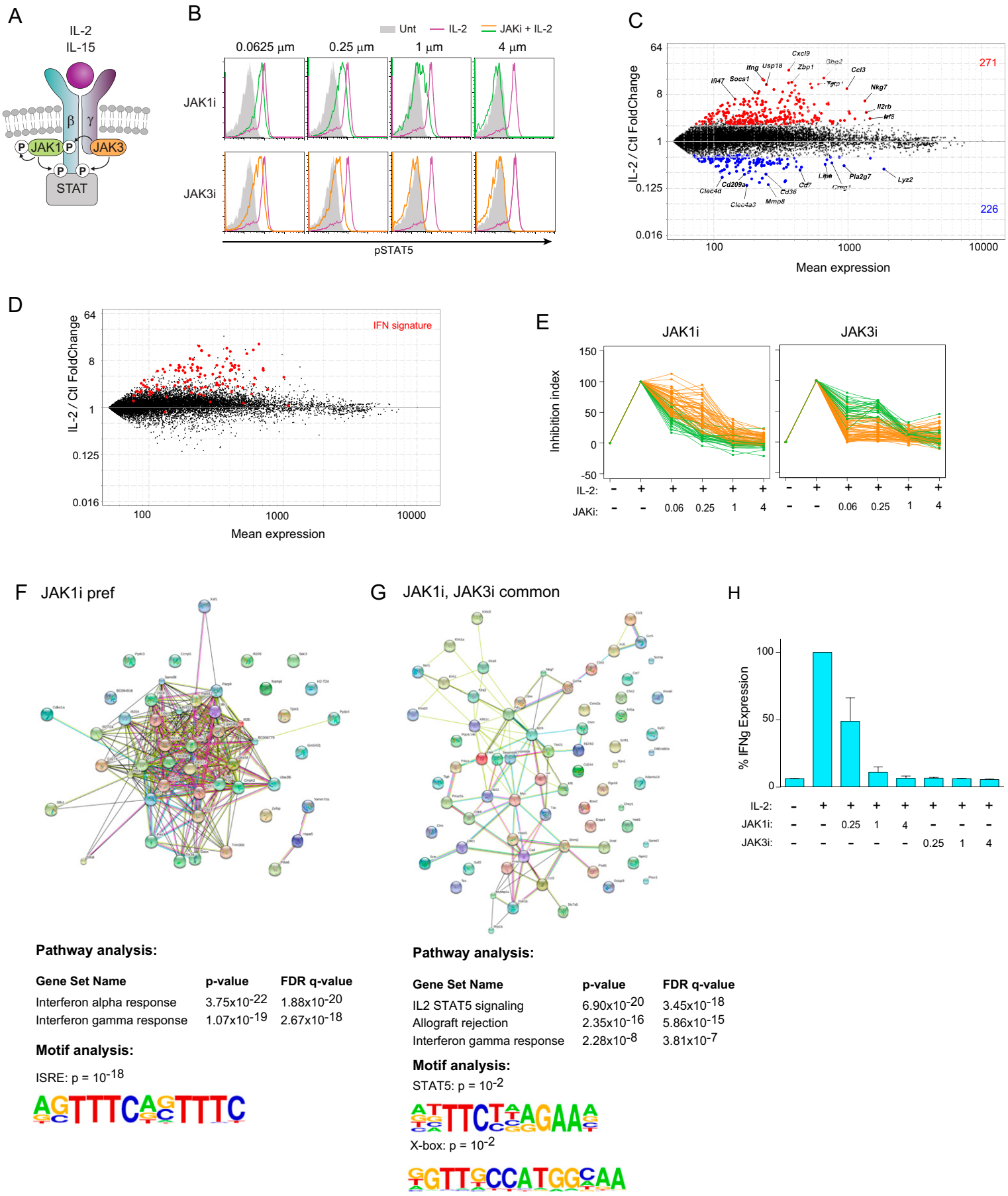

Fig. S7. The IL-2 response and effect of JAKi in NK cells. Negatively selected murine NK cells were treated with IL-2 and JAK1i or JAK3i for 8 h in vitro, and gene expression profiles were generated by microarray. (*A*) Schematic representation of the "low-affinity" IL-2Rβγ receptor complex expressed by NK cells. (*B*) Histograms showing phospho-STAT5 MFI in JAKi/IL-2–treated NK cells. (*C*) Expression vs. fold change plot showing IL-2 induced (red) and repressed (blue) genes. (*D*) Expression vs. fold change plot showing IFN signature as part of the IL-2 response. (*E*) Line graphs of JAK1i- (green) and JAK1i/JAK3i-common effects (orange) across a range of JAKi doses. (*F* and *G*) Network, pathway, and motif analyses of JAK1i-preferred (*F*) and JAK1i/JAK3i-common (*G*) IL-2 genes. Functional interactions among genes were examined by using STRING software. Pathway analysis was performed by querying hallmark gene sets in the Molecular Signatures Database (Version 5.1). Motif analysis was performed with HOMER. (*H*) Normalized *IFNg* transcript levels in JAKi/IL-2–treated NK cells.

Table S1. Enzymatic specificities of JAK inhibitors

JAK selectivity	Compound name	Compound ID	Enzyme assay IC50 (nM) @ 1 mM ATP				Mouse PBMC IC50 (nM)						
			Jak1	Jak2	Jak3	Tyk2	IL-2 (J1/3) pSTAT5	IL-15 (J1/3) pSTAT5	IL-21 (J1/3) pSTAT3	IFNa (J1/T2) pSTAT3	IL-10 (J1/T2) pSTAT3	IL-27 (J1/J2/T2) pSTAT3	IL-23 (J2/T2) pSTAT3
JAK1/JAK2	Baricitinib	PF- 6647511	4.5	7.0	601.0	50.0		12.6		3.5		3.5	26
Pan	Tofacitinib	CP-690550-10	15.1	77.4	55.0	489.0	15	15.3	21.3	9.38	42.1	8	125
JAK1	—	PF-02384554	2.75	700	>10,000	260		20.6		5.56	39.7	5.14	1,050
JAK3	—	PF-06263313	>10,000	>10,000	40	>10,000	122	116	103	9,640	>10,000	12,050	
JAK3	—	PF-06651600	>10,000	>10,000	33.1	>10,000		49.9	70.4	9,000	>10,000	>12,308	

Table S2. Antibody panels for immunophenotyping

Antibody/fluorochrome	Catalog no.	Supplier
Lymphoid panel		
TCRβ-PE-Cy7	109222	BioLegend
CD19-APC-Cy7	115530	BioLegend
TCRγδ-PerCPCy5.5	118118	BioLegend
CD4-FITC	100510	BioLegend
CD8-Alexa700	100730	BioLegend
Foxp3-APC	126408	BioLegend
Myeloid panel		
CD3-APC-Cy7	100330	BioLegend
TCRβ-APC-Cy7	109222	BioLegend
CD19-APC-Cy7	115530	BioLegend
CD11b-PerCPCy5.5	101228	BioLegend
CD11c-PE-Cy7	117318	BioLegend
F4/80-Alexa700	12310	BioLegend
Ly6c-FITC	128006	BioLegend
CD103-PE	121406	BioLegend
PDCA-1-APC	127016	BioLegend
B-cell subset panel		
CD19-APC-Cy7	115530	BioLegend
CD21-Pacific blue	123414	BioLegend
CD23-Alexa488	101609	BioLegend
IgM-APC	406509	BioLegend
IgD-PE	125993	eBioscience

Other Supporting Information Files

Dataset S1 (XLS)
Dataset S2 (XLS)
Dataset S3 (XLS)
Dataset S4 (XLS)